

Maximizing Ag Utilization in High-Rate CO₂ Electrochemical Reduction with a Coordination Polymer-Mediated Gas Diffusion Electrode

Wang, Riming; Haspel, Henrik; Pustovarenko, Alexey; Dikhtiarenko, Alla; Osadchii, Dmitrii; Ma, Ming; Smith, Wilson A.; Kapteijn, Freek; Gascon, Jorge

DOI

[10.1021/acsenergylett.9b01509](https://doi.org/10.1021/acsenergylett.9b01509)

Publication date

2019

Document Version

Accepted author manuscript

Published in

ACS Energy Letters

Citation (APA)

Wang, R., Haspel, H., Pustovarenko, A., Dikhtiarenko, A., Osadchii, D., Ma, M., Smith, W. A., Kapteijn, F., & Gascon, J. (2019). Maximizing Ag Utilization in High-Rate CO₂ Electrochemical Reduction with a Coordination Polymer-Mediated Gas Diffusion Electrode. *ACS Energy Letters*, 4(8), 2024-2031. <https://doi.org/10.1021/acsenergylett.9b01509>

Important note

To cite this publication, please use the final published version (if applicable).
Please check the document version above.

Copyright

Other than for strictly personal use, it is not permitted to download, forward or distribute the text or part of it, without the consent of the author(s) and/or copyright holder(s), unless the work is under an open content license such as Creative Commons.

Takedown policy

Please contact us and provide details if you believe this document breaches copyrights.
We will remove access to the work immediately and investigate your claim.

Maximizing Ag Utilization in High Rate CO₂ Electrochemical Reduction with a Coordination Polymer Mediated Gas Diffusion Electrode

Riming Wang, Henrik Haspel, Alexey Pustovarenko, Alla Dikhtiarenko, Artem Russkikh, Genrikh Shterk, Dmitrii Osadchii, Samy Ould-Chikh, Ming Ma, Wilson A. Smith, Kazuhiro Takanabe, Freek Kapteijn, and Jorge Gascon

ACS Energy Lett., **Just Accepted Manuscript** • DOI: 10.1021/acseenergylett.9b01509 • Publication Date (Web): 29 Jul 2019

Downloaded from pubs.acs.org on July 29, 2019

Just Accepted

“Just Accepted” manuscripts have been peer-reviewed and accepted for publication. They are posted online prior to technical editing, formatting for publication and author proofing. The American Chemical Society provides “Just Accepted” as a service to the research community to expedite the dissemination of scientific material as soon as possible after acceptance. “Just Accepted” manuscripts appear in full in PDF format accompanied by an HTML abstract. “Just Accepted” manuscripts have been fully peer reviewed, but should not be considered the official version of record. They are citable by the Digital Object Identifier (DOI®). “Just Accepted” is an optional service offered to authors. Therefore, the “Just Accepted” Web site may not include all articles that will be published in the journal. After a manuscript is technically edited and formatted, it will be removed from the “Just Accepted” Web site and published as an ASAP article. Note that technical editing may introduce minor changes to the manuscript text and/or graphics which could affect content, and all legal disclaimers and ethical guidelines that apply to the journal pertain. ACS cannot be held responsible for errors or consequences arising from the use of information contained in these “Just Accepted” manuscripts.

1
2
3
4
5
6
7 Maximizing Ag Utilization in High Rate CO₂
8
9
10
11 Electrochemical Reduction with a Coordination
12
13
14
15 Polymer Mediated Gas Diffusion Electrode
16
17
18
19

20 *Riming Wang,¹ Henrik Haspel,² Alexey Pustovarenko,² Alla Dikhtiarenko,² Artem Russkikh,²*
21 *Genrikh Shterk,² Dmitrii Osadchii,¹ Samy Ould-Chikh,² Ming Ma,³ Wilson A. Smith,³ Kazuhiro*
22 *Takanabe,^{2,4} Freek Kapteijn,¹ and Jorge Gascon*²*
23
24
25
26
27

28 1. Catalysis Engineering, Dept. of Chemical Engineering, Faculty of Applied Sciences, Delft
29 University of Technology, van der Maasweg 9, 2629 HZ Delft, The Netherlands.
30
31

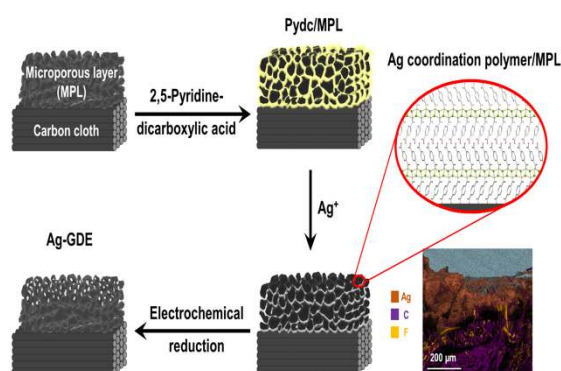
32
33
34 2. King Abdullah University of Science and Technology, KAUST Catalysis Center, Advanced
35 Catalytic Materials, Thuwal 23955, Saudi Arabia.
36
37

38
39 3. Materials for Energy Conversion and Storage (MECS), Dept. of Chemical Engineering,
40 Faculty of Applied Sciences, Delft University of Technology, Van der Maasweg 9, 2629 HZ
41 Delft, The Netherlands.
42
43
44

45
46
47 4. Department of Chemical Systems Engineering, School of Engineering, The University of
48 Tokyo, 7-3-1 Hongo, Bunkyo-ku, 113-8656, Japan.
49
50
51
52
53
54
55
56
57
58
59
60

1
2
3 ABSTRACT. We report the preparation and electrocatalytic performance of silver-containing gas
4 diffusion electrodes (GDE) derived from a silver coordination polymer (Ag-CP). Layer-by-layer
5 growth of the Ag-CP onto porous supports was applied to control Ag loading. Subsequent electro-
6 decomposition of the Ag-CP resulted in highly selective and efficient CO₂-to-CO GDE in aqueous
7 CO₂ electroreduction. Afterwards, the MOF-mediated approach was transferred to a gas-fed flow
8 electrolyzer for high-current density tests. The *in-situ* formed GDE, with a low silver loading of
9 0.2 mg cm⁻², showed a peak performance of $j_{CO} \approx 385$ mA cm⁻² at around -1.0 V vs RHE and
10 stable operation with high FE_{CO} (> 96%) at $j_{total} = 300$ mA cm⁻² over a 4 h run. These results
11 demonstrate that the MOF-mediated approach offers a facile route to manufacture uniformly
12 dispersed Ag catalysts for CO₂ER by eliminating ill-defined deposition steps (drop-casting *etc.*),
13 while allowing control of the catalyst structure through self-assembly.

TOC GRAPHICS



1
2
3 Atmospheric CO₂ concentration has been increasing drastically since the industrial revolution,
4
5
6 this has spurred different initiatives into reducing emissions and directly utilizing CO₂.¹⁻⁵ Among
7
8 the various methods proposed, CO₂ electrochemical reduction (CO₂ER) is one of the most
9
10 promising technologies due to the relatively mild operating conditions and the increasing sources
11
12 of green electricity.⁶⁻⁸ Moreover, the electrochemical reduction of CO₂ can be driven towards one
13
14 single product, avoiding expensive purification and separation steps. In this sense, the selective
15
16 electrochemical conversion of CO₂ to CO constitutes an excellent perspective technology. Au,⁹⁻¹⁰
17
18 Ag,¹¹⁻¹² and Zn¹³ have been identified as the most efficient catalysts for this process. The high price
19
20 of Au and the low stability of Zn place Ag as the most attractive option.^{12, 14-19} As it is the case in
21
22 classical heterogeneous catalysis, optimization of the final catalyst composition and metal loading
23
24 are critical to the commercialization of CO₂ER. Most studies to date have focused on the
25
26 application of metal plates^{12, 20} or supported nanoparticles^{9-11, 13, 21}. In the former case, the high metal
27
28 content per electrode area results in such high Capital Expenditures (CAPEX) that these
29
30 technologies become non-viable. Therefore, the use of supported metal catalysts seems more
31
32 realistic. Catalyst layer morphology has an effect on cathode performance: a more uniform active
33
34 phase distribution and lower particle agglomeration lead to better catalytic performance.²²
35
36 However, the fabrication of uniformly dispersed catalysts remains a significant challenge. Herein,
37
38 we propose the MOF-mediated synthesis as a facile and scalable method to manufacture highly
39
40 dispersed supported Ag catalysts with very low metal loadings for CO₂ER.
41
42
43
44
45
46

47 The use of metal-organic frameworks as catalyst precursors has gained significant attention in the
48
49 last few years.²³⁻²⁷ Following this approach, a pre-synthesized MOF is treated at high temperature
50
51 in a controlled atmosphere and transformed into a supported metal nanoparticle catalyst.²⁸ The
52
53 high activities per metal atom exhibited by the resulting catalysts, even when the total metal
54
55
56
57
58
59
60

1
2
3 content can be as high as a 50 wt%,²³ demonstrate the enormous potential of this approach. In this
4
5 work, we demonstrate that MOF mediated synthesis (MOFMS) can also be realized through
6
7 electro-decomposition.
8
9

10 Here, an Ag coordination polymer (Ag-CP) is grown directly onto carbon based microporous layer
11
12 (MPL) gas diffusion electrodes by a layer-by-layer (LBL) method, followed by the electro-
13
14 decomposition of the coordination polymer to achieve a well-defined carbon supported Ag
15
16 structure (denoted as Ag/MPL). The *in-situ* formed carbon cloth supported Ag gas diffusion
17
18 electrodes exhibit high CO₂ER efficiency in both, the traditional aqueous three-electrode system
19
20 and a gas-fed flow electrolyzer. Overcoming CO₂ transport limitations in the latter resulted in a
21
22 peak performance of $j_{CO} = 385 \text{ mA cm}^{-2}$ CO partial current density and 1864 mA mg^{-1} mass activity
23
24 due to the extremely low Ag loading. The work opens up the possibility for the direct manufacture
25
26 of CO₂ER electrodes with optimum catalyst utilization using the MOF-mediated approach.
27
28
29

30 The self-assembly between 2,5-pyridinedicarboxylic (pydc) acid and AgNO₃ in several common
31
32 solvents at room temperature leads to the formation of an Ag-CP microcrystalline powder (Table
33
34 S1-2 and Figure S1).²⁹ The crystal structure of Ag-CP was elucidated from powder X-ray
35
36 diffraction (PXRD) data by means of simulated annealing procedure followed by Rietveld
37
38 refinement.³⁰⁻³² The Ag-CP crystallizes in orthorhombic *Pbn*2₁ space group (Figure S2-3, Table
39
40 S3) and reveals a layered arrangement of silver atoms coordinated to 2,5-pydc ligands (Figure S4,
41
42 Table S4). The linker moieties lie on both sides of the Ag ion double layer: one carboxylic group
43
44 is bonded to three crystallographically equivalent silver atoms exhibiting a μ_3 -bridging mode;
45
46 another one is protonated and participates in the formation of hydrogen bonds between two Ag-
47
48 CP 2D networks (Figure 1a-c and Figure S5).
49
50
51
52
53
54
55
56
57
58
59
60

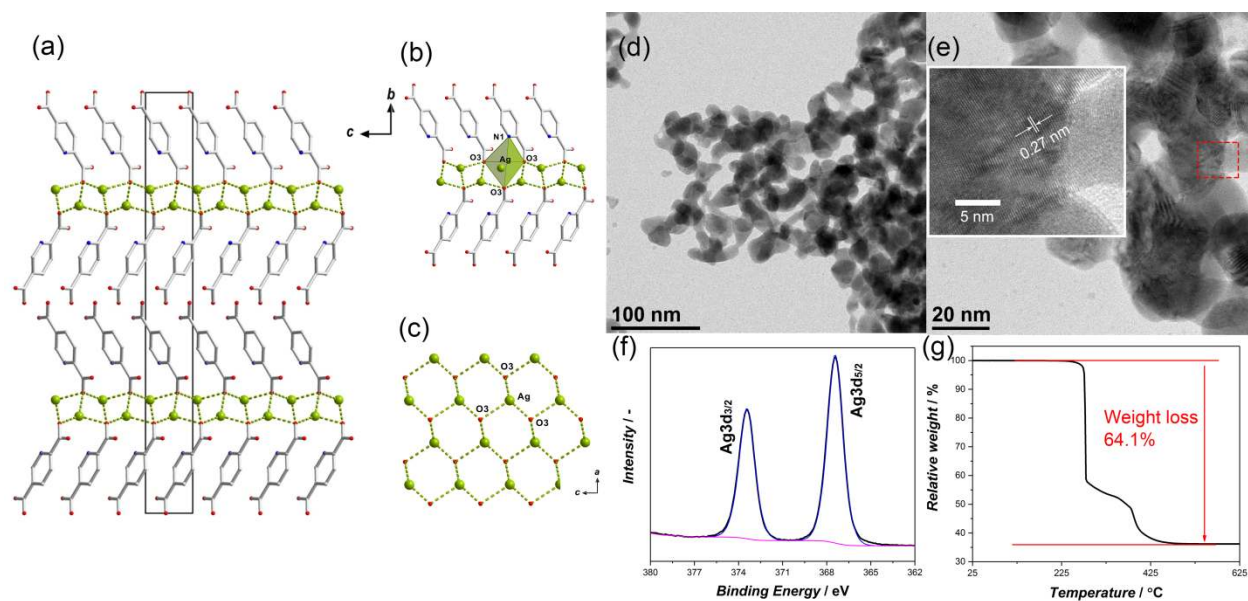


Figure 1. (a) Representation of the lamellar crystal packing and the unit cell of Ag-CP viewed along the a-axis. (b) Coordination mode of 2,5-pyridinedicarboxylic acid (μ_3 -bridging through O3 atom). (c) Hexagonal arrangement of Ag in the polymeric layer. Color scheme of the atoms: silver – green, carbon – grey, oxygen – red, nitrogen – blue. Hydrogen atoms are omitted for clarity. (d) Low-, and (e) high-magnification TEM images of Ag-CP (inset in e is a magnified image of the red box area). (f) XPS Ag3d regional spectrum of Ag-CP, and (g) TGA curve of Ag-CP in air.

Characterization results of Ag-CP are displayed in Figure 1d-g. The Ag-CP particles have a particle size ranging from 25 nm to 35 nm (Figure 1d). The high-magnification TEM image (inset of Figure 1e) shows well-defined *d*-spacing with a distance of ~ 0.27 nm. Ag3d XPS spectrum of Ag-CP (Figure 1f) exhibits two highly symmetric peaks with binding energies of 367.4 eV and 373.4 eV, corresponding to Ag3d_{5/2} and Ag3d_{3/2} photoelectron lines, respectively. Photoelectron shift of Ag3d line reveals that only oxidized Ag is present in the sample, which agrees with the Ag-O interaction in the crystal structure. Survey XPS spectrum of Ag-CP (Figure S6) proves the presence of Ag, C, N and O in the sample, and the atomic content of each element is summarized

in Table S5. The TGA curve of Ag-CP (Figure 1g) exhibits a total weight loss of $\sim 64.1\%$. Since Ag_2O is thermodynamically unfavorable at high temperature,³³ the final product is metallic Ag with a silver content of $\sim 35.9\%$. The formation of metallic Ag after the high-temperature calcination of Ag-CP in air can also be confirmed by XRD (Figure S7). N_2 physisorption of Ag-CP (Figure S8) shows a type II isotherm and absence of microporosity.

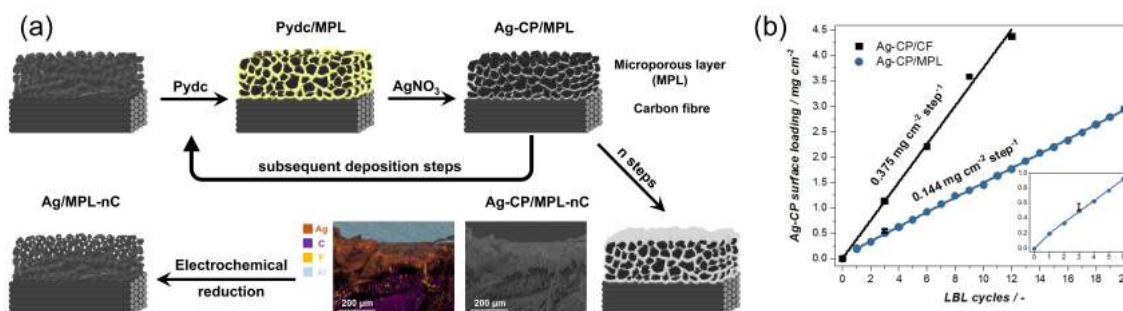


Figure 2. Scheme of the preparation of Ag/MPL catalysts, sequential deposition of Ag-CP *via* alternating adsorption of the dicarboxylic linker and the metal node and cross-sectional elemental maps of C, F, Ag and Al (a). Fluorine can be found on the PTFE-treated carbon fabric, while Al signal comes from the sample holder. Surface loading as a function of deposition steps on bare carbon fibre and MPL/carbon cloth (b). The error bar at the 3 LBL point was determined from 8 different samples.

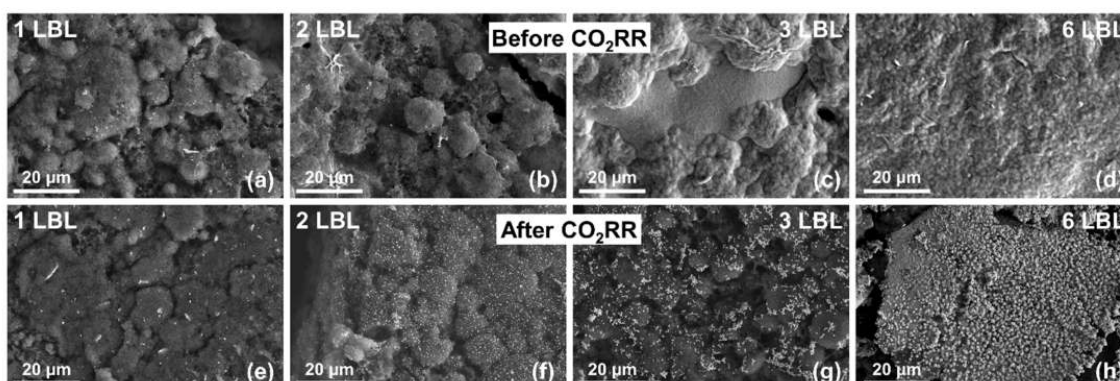
Ag-CP was deposited onto the support by the subsequent adsorption of pydc and Ag^+ from their DMF solutions (Figure 2a). The Ag-CP loading increases strictly linearly from the 2. deposition step (LBL cycle) up to 12 or 20 cycles, as it is seen in Figure 2b for bare carbon fibre and MPL containing carbon cloth alike. Utilizing the top part of the microporous layer, however, helps to achieve good surface coverage at lower Ag-CP loading ($0.144 \leftrightarrow 0.375 \text{ mg cm}^{-2} \text{ step}^{-1}$). Taking the theoretical density of the unit cell (2.557 g cm^{-3}) from Table S3 into consideration, a $0.563 \mu\text{m}$ thick Ag-CP layer - and since the longest cell parameter is around 3.2 nm , practically 150-200 unit

1
2
3 cell thickness is deposited in each cycle onto the MPL support. The higher-than-linear deposition
4
5 in the 1. LBL cycle (Figure 2b inset) is due to the high surface area of the carbon grains in the
6
7 MPL, as first the Ag-CP is built up directly onto the carbon surface (see EDS elemental maps of a
8
9 20 LBL sample in Figure 2a and S9). The actual CO₂ER catalyst is then formed by the in-situ
10
11 electrochemical reduction of the supported coordination polymer (Figure 2a). The final Ag loading
12
13 also changes linearly with the number of deposition steps as it is seen in the bare carbon fibre
14
15 based samples (Ag/CF-nC, n = 3,6,9,12) in Figure S10. The difference between the Ag-CP and Ag
16
17 loading was ~35.2 wt%, which is in good agreement with the Ag content in the crystallographically
18
19 determined formula (39.4 wt%) and with the previous TGA analysis (~35.9 wt%).
20
21
22

23
24 Although several MOF-derived electrocatalysts have been reported in the literature lately, to the
25
26 best of our knowledge, no detailed mechanistic description of the electrochemical reduction and
27
28 transformation of MOFs into the resulting NPs exists. We propose, that as the reducing potential
29
30 is applied to the electrode and the metal node is reduced back to zero valence silver, the linker
31
32 molecules are not able to coordinate and hence maintaining the continuous polymeric structure
33
34 anymore. The collapsing structure releases silver atoms at the surface of the support, and
35
36 nanoparticles and – with increasing Ag-CP coverage – agglomerated silver network are formed
37
38 through conventional aggregation.
39
40
41

42
43 According to the SEM images (Figure 3 and Figure S11-14), Ag-CP fully covers the MPL of the
44
45 gas diffusion electrode after at least 2 LBL cycles (Figure 3a-d). A spot of Ag-CP on the 1 LBL
46
47 sample is clearly seen in Figure S11a, whereas in Figure S12a-14a the CP coverage is continuous.
48
49 The subsequent electro-decomposition of Ag-CP resulted in well-dispersed of Ag nanoparticles
50
51 (Figure 3e-h) due to the homogeneous distribution of the Ag-CP precursor. The Ag/MPL-1C
52
53 electrode (Figure 3e) has a relatively sparse distribution of Ag particles, while Ag/MPL-6C shows
54
55
56
57
58
59
60

1
2
3 an agglomerated network of silver structures. Well-dispersed individual Ag particles were
4 obtained by using 2 and 3 LBL cycles (Figure 3f-g). Although the thick carbon fabric supported
5 Ag NPs are not suitable for TEM investigation, we removed the MPL grains by ultrasonication
6 and the Ag particle size distributions were determined (Figure S15). Since no significant
7 differences in the PSDs were found, we propose that there is no direct connection between
8 variation of activity and particle size in our system.
9
10
11
12
13
14
15
16



17
18
19
20
21
22
23
24
25
26
27
28
29
30 **Figure 3.** SEM images of electrodes prepared with 1 (a, e), 2 (b, f), 3 (c, g) and 6 (d, h) LBL cycles
31 before and after electro-decomposition.
32
33
34
35
36
37

38 After the L-B-L growth process, the PXRD pattern of the carbon cloth-supported Ag-CP is
39 compared with the simulated pattern of the pure Ag-CP in Figure S16a. The sharp reflections
40 demonstrate good crystallinity of Ag-CP. The position of the Ag-CP/CF reflections corresponds
41 well to those of the simulated material. After the electro-decomposition process, metallic Ag is
42 formed (Figure S16b), with three major reflections centered at 44.6°, 52.5°, and 77.2°
43 corresponding to the (111), (200), and (220) crystal facets of metallic Ag. The broad peak centered
44 at ~27° is likely to be generated by the amorphous carbon in the carbon support. And after CO₂ER,
45 the metallic Ag pattern is maintained, demonstrating the stability of the electrode.
46
47
48
49
50
51
52
53
54
55
56
57
58
59
60

1
2
3 Evolution of Ag chemical states in the sample before and after *in-situ* catalyst formation (i.e., in
4 CO₂ electrolysis) were determined by XPS (Figure S17). After deconvolution, two doublets can
5
6 be distinguished in the Ag3d line, corresponding to metallic Ag (red peaks in Figure S17 centered
7
8 at 374.2 eV and 368.2 eV) and Ag₂O (blue peaks centered at 373.6 eV and 367.6 eV).^{12,34} The ratio
9
10 of metallic Ag: oxidized Ag increases from 2.4 to 6 after one CO₂ER performance test, indicating
11
12 the reduction of Ag₂O during this process.
13
14
15

16
17 In order to demonstrate the advantage of the LBL method over drop-casting, a carbon fiber (CF)
18
19 supported Ag-CP electrode was prepared via the L-B-L method and the widely-used drop-casting
20
21 (DC) method (Scheme S1). When drop-casted, the Ag-CP particles spread around the carbon
22
23 fibres, filling the space in between them (Figure S18a,b). After electro-decomposition, large
24
25 flower-like Ag particles grow onto the fibres, leaving a large part of the carbon support uncoated
26
27 (Figure S18c,d). By comparison, the L-B-L method with 9 cycles produced uniformly dispersed
28
29 Ag-CP (Figure S18e,f) and Ag particles (Figure S18g,h) fully covering the surface of carbon fibers.
30
31 Chronoamperometric (i.e., controlled-potential) electrochemical CO₂ reduction tests were carried
32
33 out in a traditional two-compartment aqueous cell in a 0.1 M KHCO₃ electrolyte using a Pt counter
34
35 electrode. The CO₂ electroreduction performance of Ag/MPL-nC electrodes is presented in Figure
36
37 4. Only CO and H₂ were detected as products by gas and liquid chromatography (GC and UPLC),
38
39 and all the catalysts show stable CO₂ER performance after an initial 15 min period, where the *in-*
40
41 *situ* formation of the Ag/MPL takes place *via* electro-decomposition (Figure S19).
42
43
44
45

46
47 As shown in Figure 4a, the total geometrical current density increases with increasing cathode
48
49 potential ($j_{Total, max} \approx 43-44 \text{ mA cm}^{-2}$ at around -1.05 V vs. RHE for Ag/MPL-3,6C) along with the
50
51 steady increase in the FE_{CO} (Figure 4b), reaching a maximum FE_{CO} of 90-95% ($FE_{H_2} = 10-5\%$)
52
53 between -0.6 and -1.1 V vs RHE for the Ag/MPL-1,2,3C electrodes. The number of LBL cycles
54
55
56
57
58
59
60

1
2
3 also plays an important role in electrode performance with 3 cycles showing the optimal
4 compromise between the wide potential window for high FE_{CO} and the high j_{CO} (~ 30 mA cm $^{-2}$ at
5
6 -1.0 V vs. RHE) at a minimum Ag loading (Figure 4c and Table S6).
7
8

9
10 In order to investigate if the presence of linker molecules and Ag in the electrolyte solution affects
11
12 CO_2 ER performance, electrolysis were carried out at -2.0 and -1.6 V vs SCE using fresh
13
14 electrolyte right after the in-situ formation of the Ag/MPL-3C catalyst from the Ag-CP/MPL-3C
15
16 precursor (Figure S20). No significant change in the product distribution was seen, however, the
17
18 total current density drops by 15-25% after the change of the solution. We speculate that this is
19
20 due to the loss of Ag from the surface rinsing the electrode. The long-term stability of the CO_2 ER
21
22 performance was also tested using the Ag/MPL-3C sample in a refreshed electrolyte solution, and
23
24 stable CO_2 -to-CO activity was attained in a 5-hour electrolysis (Figure S21). The CO_2 ER
25
26 performance of the Ag/MPL-3C electrode was compared to similar Ag catalysts reported in the
27
28 literature (Table S7).^{12, 14-19, 35}
29
30
31
32
33
34
35
36
37
38
39
40
41
42
43
44
45
46
47
48
49
50
51
52
53
54
55
56
57
58
59
60

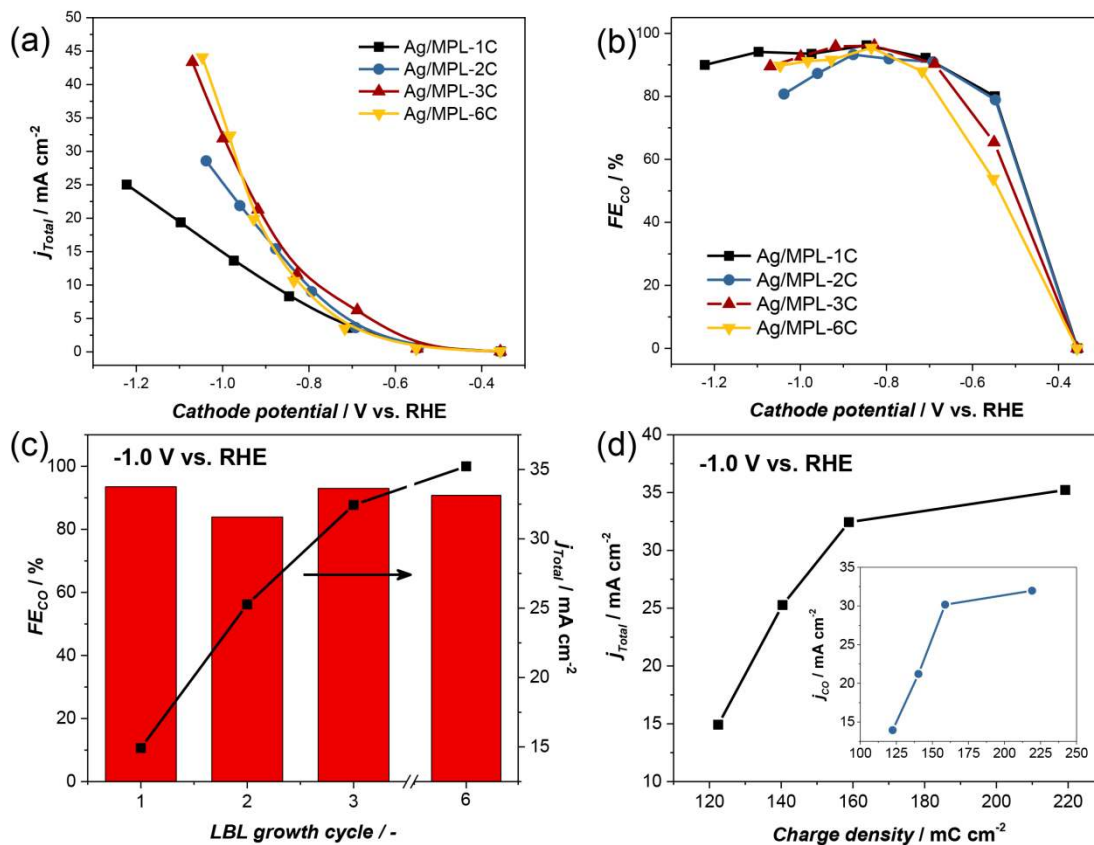


Figure 4. CO₂ electrochemical reduction performance of Ag/MPL-nC electrodes. (a) Total current density, (b) FE for CO, and (c) their LBL cycle dependency at -1.0 V vs RHE. (d) Variation of j_{Total} and j_{CO} with the electrochemical active surface area (EASA) at the same potential.

In order to address the increased j_{Total} and j_{CO} , the electrochemical active surface area (EASA) of the Ag-CP and Ag/MPL-nC samples was determined by the monolayer silver oxide method in 0.1 M KOH.³⁵⁻³⁶ The charge for monolayer oxide formation was calculated in Figure S22. EASA almost linearly increases with ongoing LBL cycles (Figure S23), which then does not accompanied by the same increase in the total and CO current density. The latter levels off at 3 deposition cycles (Figure 4d). Even though the total amount of silver in Ag/MPL-6C increased considerably compared to Ag/MPL-3C (twice as many LBL cycles), it is not accompanied by the increase in

1
2
3 the number of accessible active sites. The effect of electro-decomposition, i.e., the formation of
4 Ag particles can be followed in Figure S23. The EASA saturates after 2 LBL cycles at a lower
5 level, as the increase in Ag loading (in the form of Ag-CP) is not followed by an increase of the
6 number of active sites, demonstrating that only Ag in the outer surface acts as a CO₂-to-CO
7 electrocatalyst.
8
9

10 CO₂ mass transport limitations are the bottleneck that prevent achieving high current densities in
11 aqueous phase CO₂ electrolysis.³⁷⁻³⁸ Therefore, we turned to a gas-fed flow electrolyzer to perform
12 high current density chronopotentiometric CO₂ electrolysis on the Ag/MPL-3C electrode.³⁹⁻⁴⁵ The
13 cathode side was fed by a humidified CO₂ stream without using any liquid catholyte, and a nickel
14 mesh was used as an oxygen evolution catalyst in recirculated 1 M KOH anolyte at the anode side.
15
16 The two compartments were separated by Sustainion S-50 polyimidazolium-based anion exchange
17 membrane. The catalytically active Ag particles were *in-situ* formed from the pre-synthesized Ag-
18 CP *via* an initial chronoamperometric run at constant -2 V *vs* Hg/HgO potential under CO₂
19 electroreduction conditions (Figure S24). CO was formed with high selectivity right from the
20 beginning of the activation step, and j_{CO} levels off after about 20 min at typically around 200-300
21 mA cm⁻².
22
23
24
25
26
27
28
29
30
31
32
33
34
35
36
37
38
39
40
41
42
43
44
45
46
47
48
49
50
51
52
53
54
55
56
57
58
59
60

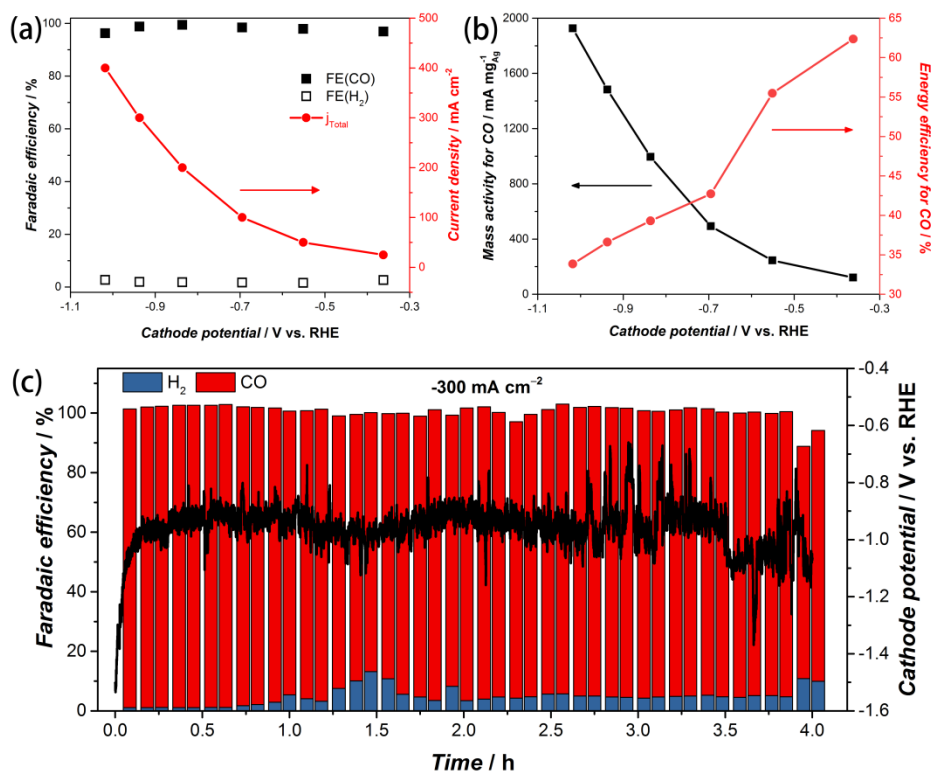


Figure 5. CO₂ER performance of the Ag/MPL-3C electrode in a gas-fed zero gap flow electrolyzer. (a) Faradaic efficiency and total current density, and (b) mass activity energy efficiency for CO. (c) Stability test at -300 mA cm^{-2} for 4 h, the bar diagram represents the FE (left y-axis) of CO (red) and H₂ (blue), and the black line represents the cathode potential (right y-axis).

Immediately after the initial CA run, chronopotentiometric CO₂ electrolysis was done at different current densities. A moderately high current density of -25 mA cm^{-2} was achieved at a cathode potential of around -0.36 V vs RHE (Figure 5a). Towards higher current densities the cathode potential climbed to -1.04 V vs. RHE , which corresponds to a cell voltage of 3.78 V , at $j_{\text{Total}} = -400 \text{ mA cm}^{-2}$. High FE_{CO} ($> 96\%$) was achieved in the whole tested current density range, peaking at $FE_{\text{CO}} = 99.5\%$ at $j_{\text{Total}} = -200 \text{ mA cm}^{-2}$ ($E_{\text{Cathode}} = -0.84 \text{ V vs. RHE}$). The flow cell CO₂ER

1
2
3 performance of the Ag/MPL-3C catalyst are summarized in Table S8, and compared to literature
4 data on high current density flow cell CO₂-to-CO electrolysis (Table S9, Figure S25a).^{16, 46-58}

7 Active phase dispersion and accessibility plays a crucial role in catalytic performance. To this end,
8 the MOF mediated synthesis, combined with electro-decomposition, offers a straightforward
9 approach to achieving high mass activity of the catalyst. In Ag/MPL-3C the Ag-CP and Ag loading
10 are 0.55 mg cm⁻² and 0.20-0.21 mg cm⁻², respectively, which in turn results in a mass activity of
11 1864-1926 mA mg_{Ag}⁻¹ (Figure 5b), one of the highest values ever reported (Table S9, Figure
12 S25b).^{16, 46-58} The energy efficiency of CO formation remains above 50% at moderate current
13 densities (< 100 mA cm⁻²), and drops to the 32-42% range during high current density operation
14 due to the elevated cell potential (Figure 5b). The main source of the low energy efficiencies is
15 either the high overvoltage (energy wasted as dissipated heat) and/or low CO selectivity (energy
16 wasted as undesired products).³⁷

17 Ag/MPL-3C showed stable high current density performance at -300 mA cm⁻² for 4 h (Figure 5c).
18 The estimated average potential was -0.94 V vs RHE in the first 3.5 h. The fluctuation in the
19 potential reading is due to the intensive bubble formation at the nickel mesh anode catalyst, as the
20 counter electrode potential was directly determined in this setup. The cell potential oscillated at
21 around 3.2 V in the first 3 h, then it shifted to higher voltages (Figure S26). Moreover, gas flow
22 fluctuation due to carbonate precipitation in the cathode flow channels is a further issue to be
23 solved in industrial scale high rate operations in alkaline environment CO₂ electrolysis.^{37, 50} Images
24 of a crystalline precipitate is seen after a long-term electrolysis in Figure S27 without (a) and with
25 (b) reactant stream humidification, its XRD pattern (Figure S28) shows that mainly KHCO₃ was
26 formed in the flow channels and on the macroporous side of the carbon cloth GDE. The temporary
27 increase in FE_{H_2} at around 1.5 h is most probably the result of the building-up of the KHCO₃ layer
28
29
30
31
32
33
34
35
36
37
38
39
40
41
42
43
44
45
46
47
48
49
50
51
52
53
54
55
56
57
58
59
60

1
2
3 on the cathode side of the cell. This on one hand, partly blocks the CO₂ flow, but on the other hand
4 provides a suitable environment for CO₂ER as HCO₃⁻ ion layer at the cathode is known for
5 stabilizing the CO₂ER performance in flow electrolyzers.^{37,50}
6
7

8
9
10 In summary, the MOF-mediated approach, *i.e.*, LBL deposition of Ag-CP followed by electro-
11 decomposition, offers a facile route to manufacture uniformly dispersed Ag catalysts for CO₂ER.
12
13 In spite of the small amount of Ag in the final electrodes (0.2 mg cm⁻²), gas diffusion electrodes
14 show excellent CO₂ER performance in traditional aqueous cells ($FE_{CO} \approx 90-95\%$ and $j_{CO,max} = 38.8$
15 mA cm⁻² at -1.07 V vs RHE) and in a gas-fed electrolyzer ($j_{CO,max} = 385$ mA cm⁻² at -1.04 V vs.
16 RHE). The enhanced catalyst dispersion and utilization resulted in one of the highest silver mass
17 activities (1864 mA mg_{Ag}⁻¹) in the literature to date. The direct synthesis of metal electrocatalyst
18 eliminates the need for ill-defined deposition steps (drop-casting *etc.*), while allowing tight control
19 of the catalyst structure through self-assembly.
20
21
22
23
24
25
26
27
28
29
30
31
32
33
34
35
36
37
38
39
40
41
42
43
44
45
46
47
48
49
50
51
52
53
54
55
56
57
58
59
60

1
2
3 ASSOCIATED CONTENT
4
5

6 **Supporting Information.** Optimization of the synthetic conditions. Crystal structure details.
7
8 Experimental details. Figures of material characterization, including SEM, XRD, and XPS.
9
10
11 Additional CO₂ electroreduction performance.
12
13

14 AUTHOR INFORMATION
15
16

17 **Corresponding Author**
18

19
20 * E-mail: jorge.gascon@kaust.edu.sa.
21
22

23 **Notes**
24

25 The authors declare no competing financial interest.
26
27

28 ACKNOWLEDGMENT
29
30

31 The authors would like to thank China Scholarship Council (CSC) and TOTAL for the financial
32
33 support.
34
35
36
37
38
39
40
41
42
43
44
45
46
47
48
49
50
51
52
53
54
55
56
57
58
59
60

REFERENCES

1. Kondratenko, E. V.; Mul, G.; Baltrusaitis, J.; Larrazabal, G. O.; Perez-Ramirez, J., Status and perspectives of CO₂ conversion into fuels and chemicals by catalytic, photocatalytic and electrocatalytic processes. *Energ Environ Sci* **2013**, *6* (11), 3112-3135.
2. Saeidi, S.; Amin, N. A. S.; Rahimpour, M. R., Hydrogenation of CO₂ to value-added products-A review and potential future developments. *Journal of Co2 Utilization* **2014**, *5*, 66-81.
3. Sharma, S.; Hu, Z. P.; Zhang, P.; McFarland, E. W.; Metiu, H., CO₂ methanation on Ru-doped ceria. *Journal of Catalysis* **2011**, *278* (2), 297-309.
4. Thampi, K. R.; Kiwi, J.; Gratzel, M., Methanation and Photo-Methanation of Carbon-Dioxide at Room-Temperature and Atmospheric-Pressure. *Nature* **1987**, *327* (6122), 506-508.
5. Wang, W.; Wang, S.; Ma, X.; Gong, J., Recent advances in catalytic hydrogenation of carbon dioxide. *Chem Soc Rev* **2011**, *40* (7), 3703-27.
6. Whipple, D. T.; Kenis, P. J. A., Prospects of CO₂ Utilization via Direct Heterogeneous Electrochemical Reduction. *J Phys Chem Lett* **2010**, *1* (24), 3451-3458.
7. Lu, Q.; Jiao, F., Electrochemical CO₂ reduction: Electrocatalyst, reaction mechanism, and process engineering. *Nano Energy* **2016**, *29*, 439-456.
8. Ganesh, I., Electrochemical conversion of carbon dioxide into renewable fuel chemicals - The role of nanomaterials and the commercialization. *Renew Sust Energ Rev* **2016**, *59*, 1269-1297.
9. Zhu, W.; Michalsky, R.; Metin, O.; Lv, H.; Guo, S.; Wright, C. J.; Sun, X.; Peterson, A. A.; Sun, S., Monodisperse Au nanoparticles for selective electrocatalytic reduction of CO₂ to CO. *J Am Chem Soc* **2013**, *135* (45), 16833-6.
10. Mistry, H.; Reske, R.; Zeng, Z.; Zhao, Z. J.; Greeley, J.; Strasser, P.; Cuenya, B. R., Exceptional size-dependent activity enhancement in the electroreduction of CO₂ over Au nanoparticles. *J Am Chem Soc* **2014**, *136* (47), 16473-6.
11. Sastre, F.; Munoz-Batista, M. J.; Kubacka, A.; Fernandez-Garcia, M.; Smith, W. A.; Kapteijn, F.; Makkee, M.; Gascon, J., Efficient Electrochemical Production of Syngas from CO₂ and H₂O by using a Nanostructured Ag/g-C₃N₄ Catalyst. *Chemelectrochem* **2016**, *3* (9), 1497-1502.
12. Ma, M.; Trzesniewski, B. J.; Xie, J.; Smith, W. A., Selective and Efficient Reduction of Carbon Dioxide to Carbon Monoxide on Oxide-Derived Nanostructured Silver Electrocatalysts. *Angewandte Chemie* **2016**, *55* (33), 9748-52.
13. Won da, H.; Shin, H.; Koh, J.; Chung, J.; Lee, H. S.; Kim, H.; Woo, S. I., Highly Efficient, Selective, and Stable CO₂ Electroreduction on a Hexagonal Zn Catalyst. *Angewandte Chemie* **2016**, *55* (32), 9297-300.
14. Daiyan, R.; Lu, X. Y.; Ng, Y. H.; Amal, R., Highly Selective Conversion of CO₂ to CO Achieved by a Three-Dimensional Porous Silver Electrocatalyst. *Chemistryselect* **2017**, *2* (3), 879-884.
15. Liu, S.; Tao, H.; Zeng, L.; Liu, Q.; Xu, Z.; Liu, Q.; Luo, J. L., Shape-Dependent Electrocatalytic Reduction of CO₂ to CO on Triangular Silver Nanoplates. *J Am Chem Soc* **2017**, *139* (6), 2160-2163.
16. Lu, Q.; Rosen, J.; Zhou, Y.; Hutchings, G. S.; Kimmel, Y. C.; Chen, J. G.; Jiao, F., A selective and efficient electrocatalyst for carbon dioxide reduction. *Nat Commun* **2014**, *5*, 3242.
17. Mistry, H.; Choi, Y. W.; Bagger, A.; Scholten, F.; Bonifacio, C. S.; Sinev, I.; Divins, N. J.; Zegkinoglou, I.; Jeon, H. S.; Kisslinger, K.; Stach, E. A.; Yang, J. C.; Rossmeisl, J.; Roldan

- 1
2
3 Cuenya, B., Enhanced Carbon Dioxide Electroreduction to Carbon Monoxide over Defect-Rich
4 Plasma-Activated Silver Catalysts. *Angewandte Chemie* **2017**, *56* (38), 11394-11398.
- 5 18. Peng, X.; Karakalos, S. G.; Mustain, W. E., Preferentially Oriented Ag Nanocrystals with
6 Extremely High Activity and Faradaic Efficiency for CO₂ Electrochemical Reduction to CO.
7 *ACS Appl Mater Interfaces* **2018**, *10* (2), 1734-1742.
- 8 19. Rosen, B. A.; Salehi-Khojin, A.; Thorson, M. R.; Zhu, W.; Whipple, D. T.; Kenis, P. J.;
9 Masel, R. I., Ionic liquid-mediated selective conversion of CO(2) to CO at low overpotentials.
10 *Science* **2011**, *334* (6056), 643-4.
- 11 20. Hori, Y.; Kikuchi, K.; Suzuki, S., Production of CO and CH₄ in Electrochemical
12 Reduction of CO₂ at Metal-Electrodes in Aqueous Hydrogencarbonate Solution. *Chem Lett*
13 **1985**, (11), 1695-1698.
- 14 21. Wang, R.; Sun, X.; Ould-Chikh, S.; Osadchii, D.; Bai, F.; Kapteijn, F.; Gascon, J., Metal-
15 Organic-Framework-Mediated Nitrogen-Doped Carbon for CO₂ Electrochemical Reduction.
16 *ACS Appl Mater Interfaces* **2018**, *10* (17), 14751-14758.
- 17 22. Jhong, H.-R. M.; Brushett, F. R.; Kenis, P. J. A., The Effects of Catalyst Layer
18 Deposition Methodology on Electrode Performance. *Advanced Energy Materials* **2013**, *3* (5),
19 589-599.
- 20 23. Sun, X.; Suarez, A. I. O.; Meijerink, M.; van Deelen, T.; Ould-Chikh, S.; Zecevic, J.; de
21 Jong, K. P.; Kapteijn, F.; Gascon, J., Manufacture of highly loaded silica-supported cobalt
22 Fischer-Tropsch catalysts from a metal organic framework. *Nat Commun* **2017**, *8* (1), 1680.
- 23 24. Sun, X.; Olivos-Suarez, A. I.; Osadchii, D.; Romero, M. J. V.; Kapteijn, F.; Gascon, J.,
24 Single cobalt sites in mesoporous N-doped carbon matrix for selective catalytic hydrogenation of
25 nitroarenes. *Journal of Catalysis* **2018**, *357*, 20-28.
- 26 25. Sun, X.; Olivos-Suarez, A. I.; Oar-Arteta, L.; Rozhko, E.; Osadchii, D.; Bavykina, A.;
27 Kapteijn, F.; Gascon, J., Metal-Organic Framework Mediated Cobalt/Nitrogen-Doped Carbon
28 Hybrids as Efficient and Chemoselective Catalysts for the Hydrogenation of Nitroarenes.
29 *Chemcatchem* **2017**, *9* (10), 1854-1862.
- 30 26. Santos, V. P.; Wezendonk, T. A.; Jaen, J. J.; Dugulan, A. I.; Nasalevich, M. A.; Islam, H.
31 U.; Chojecki, A.; Sartipi, S.; Sun, X.; Hakeem, A. A.; Koeken, A. C.; Ruitenbeek, M.; Davidian,
32 T.; Meima, G. R.; Sankar, G.; Kapteijn, F.; Makkee, M.; Gascon, J., Metal organic framework-
33 mediated synthesis of highly active and stable Fischer-Tropsch catalysts. *Nat Commun* **2015**, *6*,
34 6451.
- 35 27. Oar-Arteta, L.; Wezendonk, T.; Sun, X. H.; Kapteijn, F.; Gascon, J., Metal organic
36 frameworks as precursors for the manufacture of advanced catalytic materials. *Materials*
37 *Chemistry Frontiers* **2017**, *1* (9), 1709-1745.
- 38 28. Wang, R.; Kapteijn, F.; Gascon, J., Engineering Metal–Organic Frameworks for the
39 Electrochemical Reduction of CO₂: A Minireview. *Chemistry – An Asian Journal* **0** (0).
- 40 29. Lu, X.; Ye, J.; Zhang, D.; Xie, R.; Bogale, R. F.; Sun, Y.; Zhao, L.; Zhao, Q.; Ning, G.,
41 Silver carboxylate metal-organic frameworks with highly antibacterial activity and
42 biocompatibility. *J Inorg Biochem* **2014**, *138*, 114-121.
- 43 30. Pawley, G. S., Unit-Cell Refinement from Powder Diffraction Scans. *J Appl Crystallogr*
44 **1981**, *14* (Dec), 357-361.
- 45 31. Boulton, A.; Louer, D., Powder pattern indexing with the dichotomy method. *J Appl*
46 *Crystallogr* **2004**, *37*, 724-731.
- 47
48
49
50
51
52
53
54
55
56
57
58
59
60

- 1
2
3 32. Altomare, A.; Corriero, N.; Cuocci, C.; Falcicchio, A.; Moliterni, A.; Rizzi, R., EXPO
4 software for solving crystal structures by powder diffraction data: methods and application. *Cryst*
5 *Res Technol* **2015**, *50* (9-10), 737-742.
- 6 33. L'vov, B. V., Kinetics and mechanism of thermal decomposition of silver oxide.
7 *Thermochim Acta* **1999**, *333* (1), 13-19.
- 8 34. Gao, X. Y.; Wang, S. Y.; Li, J.; Zheng, Y. X.; Zhang, R. J.; Zhou, P.; Yang, Y. M.; Chen,
9 L. Y., Study of structure and optical properties of silver oxide films by ellipsometry, XRD and
10 XPS methods. *Thin Solid Films* **2004**, *455*, 438-442.
- 11 35. Ma, M.; Liu, K.; Shen, J.; Kas, R.; Smith, W. A., In Situ Fabrication and Reactivation of
12 Highly Selective and Stable Ag Catalysts for Electrochemical CO₂ Conversion. *ACS Energy*
13 *Letters* **2018**, *3* (6), 1301-1306.
- 14 36. Rosen, J.; Hutchings, G. S.; Lu, Q.; Rivera, S.; Zhou, Y.; Vlachos, D. G.; Jiao, F.,
15 Mechanistic Insights into the Electrochemical Reduction of CO₂ to CO on Nanostructured Ag
16 Surfaces. *Acs Catal* **2015**, *5* (7), 4293-4299.
- 17 37. Martín, A. J.; Larrazábal, G. O.; Pérez-Ramírez, J., Towards sustainable fuels and
18 chemicals through the electrochemical reduction of CO₂: lessons from water electrolysis. *Green*
19 *Chemistry* **2015**, *17* (12), 5114-5130.
- 20 38. Schwarz, H. A.; Dodson, R. W., Reduction potentials of CO₂- and the alcohol radicals.
21 *The Journal of Physical Chemistry* **1989**, *93* (1), 409-414.
- 22 39. Han, L.; Zhou, W.; Xiang, C., High-Rate Electrochemical Reduction of Carbon
23 Monoxide to Ethylene Using Cu-Nanoparticle-Based Gas Diffusion Electrodes. *ACS Energy*
24 *Letters* **2018**, *3* (4), 855-860.
- 25 40. Burdyny, T.; Smith, W. A., CO₂ reduction on gas-diffusion electrodes and why catalytic
26 performance must be assessed at commercially-relevant conditions. *Energy Environ Sci* **2019**.
- 27 41. Higgins, D.; Hahn, C.; Xiang, C.; Jaramillo, T. F.; Weber, A. Z., Gas-Diffusion
28 Electrodes for Carbon Dioxide Reduction: A New Paradigm. *ACS Energy Letters* **2019**, *4* (1),
29 317-324.
- 30 42. Wu, J.; Risalvato, F. G.; Sharma, P. P.; Pellechia, P. J.; Ke, F.-S.; Zhou, X.-D.,
31 Electrochemical Reduction of Carbon Dioxide. *J Electrochem Soc* **2013**, *160* (9), F953-F957.
- 32 43. Merino-Garcia, I.; Alvarez-Guerra, E.; Albo, J.; Irabien, A., Electrochemical membrane
33 reactors for the utilisation of carbon dioxide. *Chem Eng J* **2016**, *305*, 104-120.
- 34 44. Endrődi, B.; Bencsik, G.; Darvas, F.; Jones, R.; Rajeshwar, K.; Janáky, C., Continuous-
35 flow electroreduction of carbon dioxide. *Progress in Energy and Combustion Science* **2017**, *62*,
36 133-154.
- 37 45. Weekes, D. M.; Salvatore, D. A.; Reyes, A.; Huang, A.; Berlinguette, C. P., Electrolytic
38 CO₂ Reduction in a Flow Cell. *Accounts Chem Res* **2018**, *51* (4), 910-918.
- 39 46. Ma, S.; Luo, R.; Gold, J. I.; Yu, A. Z.; Kim, B.; Kenis, P. J. A., Carbon nanotube
40 containing Ag catalyst layers for efficient and selective reduction of carbon dioxide. *J Mater*
41 *Chem A* **2016**, *4* (22), 8573-8578.
- 42 47. Ma, S.; Luo, R.; Moniri, S.; Lan, Y.; Kenis, P. J. A., Efficient Electrochemical Flow
43 System with Improved Anode for the Conversion of CO₂ to CO. *J Electrochem Soc* **2014**, *161*
44 (10), F1124-F1131.
- 45 48. Ma, S.; Lan, Y.; Perez, G. M. J.; Moniri, S.; Kenis, P. J. A., Silver Supported on Titania
46 as an Active Catalyst for Electrochemical Carbon Dioxide Reduction. *ChemSusChem* **2014**, *7*
47 (3), 866-874.
- 48
49
50
51
52
53
54
55
56
57
58
59
60

- 1
2
3 49. Tornow, C. E.; Thorson, M. R.; Ma, S.; Gewirth, A. A.; Kenis, P. J. A., Nitrogen-Based
4 Catalysts for the Electrochemical Reduction of CO₂ to CO. *Journal of the American Chemical*
5 *Society* **2012**, *134* (48), 19520-19523.
- 6 50. Verma, S.; Hamasaki, Y.; Kim, C.; Huang, W.; Lu, S.; Jhong, H.-R. M.; Gewirth, A. A.;
7 Fujigaya, T.; Nakashima, N.; Kenis, P. J. A., Insights into the Low Overpotential
8 Electroreduction of CO₂ to CO on a Supported Gold Catalyst in an Alkaline Flow Electrolyzer.
9 *ACS Energy Letters* **2018**, *3* (1), 193-198.
- 10 51. Verma, S.; Lu, X.; Ma, S.; Masel, R. I.; Kenis, P. J. A., The effect of electrolyte
11 composition on the electroreduction of CO₂ to CO on Ag based gas diffusion electrodes.
12 *Physical Chemistry Chemical Physics* **2016**, *18* (10), 7075-7084.
- 13 52. Dinh, C.-T.; García de Arquer, F. P.; Sinton, D.; Sargent, E. H., High Rate, Selective, and
14 Stable Electroreduction of CO₂ to CO in Basic and Neutral Media. *ACS Energy Letters* **2018**, *3*
15 (11), 2835-2840.
- 16 53. Haas, T.; Krause, R.; Weber, R.; Demler, M.; Schmid, G., Technical photosynthesis
17 involving CO₂ electrolysis and fermentation. *Nature Catalysis* **2018**, *1* (1), 32-39.
- 18 54. Jhong, H.-R. M.; Tornow, C. E.; Kim, C.; Verma, S.; Oberst, J. L.; Anderson, P. S.;
19 Gewirth, A. A.; Fujigaya, T.; Nakashima, N.; Kenis, P. J. A., Gold Nanoparticles on Polymer-
20 Wrapped Carbon Nanotubes: An Efficient and Selective Catalyst for the Electroreduction of
21 CO₂. *Chemphyschem* **2017**, *18* (22), 3274-3279.
- 22 55. Jhong, H.-R. M.; Tornow, C. E.; Smid, B.; Gewirth, A. A.; Lyth, S. M.; Kenis, P. J. A., A
23 Nitrogen-Doped Carbon Catalyst for Electrochemical CO₂ Conversion to CO with High
24 Selectivity and Current Density. *ChemSusChem* **2017**, *10* (6), 1094-1099.
- 25 56. Kim, B.; Hillman, F.; Ariyoshi, M.; Fujikawa, S.; Kenis, P. J. A., Effects of composition
26 of the micro porous layer and the substrate on performance in the electrochemical reduction of
27 CO₂ to CO. *J Power Sources* **2016**, *312*, 192-198.
- 28 57. Ma, S.; Liu, J.; Sasaki, K.; Lyth, S. M.; Kenis, P. J. A., Carbon Foam Decorated with
29 Silver Nanoparticles for Electrochemical CO₂ Conversion. *Energy Technology* **2017**, *5* (6), 861-
30 863.
- 31 58. Möller, T.; Ju, W.; Bagger, A.; Wang, X.; Luo, F.; Ngo Thanh, T.; Varela, A. S.;
32 Rossmesl, J.; Strasser, P., Efficient CO₂ to CO electrolysis on solid Ni–N–C catalysts at
33 industrial current densities. *Energ Environ Sci* **2019**, *12* (2), 640-647.
- 34
35
36
37
38
39
40
41
42
43
44
45
46
47
48
49
50
51
52
53
54
55
56
57
58
59
60